Optical Properties of Humic Substances and CDOM: Relation to Structure

ARTICLE *in* ENVIRONMENTAL SCIENCE AND TECHNOLOGY · MAY 2009

Impact Factor: 5.33 · DOI: 10.1021/es803264g · Source: PubMed

5 AUTHORS, INCLUDING:

Rossana Del Vecchio
University of Maryland, College Park
23 PUBLICATIONS **1,271** CITATIONS

SEE PROFILE

Article

Optical Properties of Humic Substances and CDOM: Relation to Structure

Erin S. Boyle, Nicolas Guerriero, Anthony Thiallet, Rossana Del Vecchio, and Neil V. Blough

Environ. Sci. Technol., **2009**, 43 (7), 2262-2268• Publication Date (Web): 02 March 2009

Environ. Sci. Technol. **2009,** *43,* 2262–2268

Optical Properties of Humic Substances and CDOM: Relation to Structure

ERIN S. BOYLE,[†] NICOLAS GUERRIERO,[†] ANTHONY THIALLET,[†] ROSSANA DEL VECCHIO,*[,‡] AND NEIL V. BLOUGH*[,†]

Department of Chemistry and Biochemistry, University of Maryland, College Park, Maryland 20742, and Earth System Science Interdisciplinary Center, University of Maryland, College Park, Maryland 20742

Received November 20, 2008. Revised manuscript received January 30, 2009. Accepted February 3, 2009.

The spectral dependencies of absorption and fluorescence emission (emission maxima (λ_{max}), quantum yields (ϕ), and mean lifetimes (τ_m)) were acquired for a commercial lignin, Suwannee River humic (SRHA) and fulvic (SRFA) acids, and a series solid phase extracts (C18) from the Middle Atlantic Bight (MAB extracts). These parameters were compared with the relative average size and total lignin phenol content (TLP). TLP was strongly correlated with absorption at 280 and 355 nm for the MAB extracts, SRHA, and SRFA. The spectral dependence of λ_{max}, ϕ, and τ_m was very similar for all samples, suggesting a common photophysical and thus structural basis. A strong decrease of ϕ and τ_m with increasing average size indicates that intramolecular interactions must be important. When combined with previous work, the results lead us to conclude that the optical properties commonly associated with terrestrial humic substances and chromophoric dissolved organic matter arise primarily from an ensemble of partially oxidized lignins derived from vascular plant sources. They further provide additional support for an electronic interaction model in which intramolecular energy transfer, excited-state electron transfer, as well as charge transfer likely play important roles in producing the observed optical and photochemical properties of these materials.

Introduction

Although the optical properties of humic substances (HS) and chromophoric dissolved organic matter (CDOM) have been investigated for decades (*1*−*7*), the structural basis of these properties remains unclear (*3*−*8*). These materials exhibit rather unusual absorption and emission characteristics: absorption decreases with increasing wavelength in an approximately exponential fashion, but extends well into the visible and in some cases the near-infrared; emission maxima (λ_{max}) shift continuously to the red with increasing excitation wavelength ($\lambda_{ex} \geq 375$ nm) while the fluorescence quantum yields (ϕ) monotonically decrease. These results provide exceedingly strong evidence that the absorption and emission spectra must arise from a very large number of absorbing and emitting species or states (*8, 9*). However, previous results indicate that the spectra cannot result solely from a simple linear sum of the spectra of numerous independently absorbing and emitting chromophores, but instead that intramolecular electronic interactions between chromophores must also be playing an important role (*8*). Based on this study (*8*), as well as others (*10*−*22*), the optical properties of humic substances were proposed to result in part from intramolecular charge-transfer interactions between hydroxy-aromatic donors and quinoid (or other) acceptors formed through the partial oxidation of lignin and possibly other polymeric hydroxy-aromatic precursors (*8*).

To gain further insight into the structural basis of HS optical properties, the spectral dependence of the fluorescence emission maxima, quantum yields, and lifetimes (τ) of a commercial lignin, Suwannee River fulvic (SRFA) and humic (SRHA) acids, and a series of samples obtained from diverse natural waters through solid phase extraction (C18) were compared. The data obtained from these measurements were further compared with the relative average molecular size and total lignin phenol content. The results provide additional support for an electronic interaction model in which intramolecular energy transfer, excited-state electron transfer, as well as charge transfer likely play important roles in producing the observed optical and photochemical properties of HS, CDOM, and extracted (partially oxidized) lignins.

Materials and Methods

Reagents. Water was obtained from a Millipore Milli-Q Plus purification system. SRFA and SRHA were obtained from the International Humic Substances Society. Na_2HPO_4 and NaH_2PO_4 used for buffer solution were obtained from J.T. Baker. Alkali-extracted carboxylated lignin (LAC) was acquired from Aldrich (lot no. 19714 DS). As reported by Aldrich, the weight average (M_w) and number average (M_n) molecular weight of LAC is ∼175 000 and ∼16 000, respectively.

Extracted Samples. Natural waters (CDOM) and extracts (C18) were obtained from samples (20 L) collected onboard the research vessel R/V Cape Henlopen or the R/V Hugh Sharp in the Middle Atlantic Bight (MAB) along a transect from the Delaware River to the western boundary of the Gulf Stream during two summer cruises (September 2005 and August 2006) (Table 1): mid Delaware Bay, 2 m, 1_MDB_2m_(06) or 6_MDB_2m_(05); continental shelf, 2 m, 2_Shelf_2m_(06) or 7_Shelf_2m_(05); continental shelf, 35 or 43 m, 3_Shelf_35m_(06) or 8_Shelf_43m_(05); Gulf Stream, 2 m, 4_GS_2m_(06); and Gulf Stream, 1000 m, 5_GS_1000m_(06). Water samples were first filtered (0.2 μm Gellman filter), acidified to pH 2 and pumped through the solvent phase extraction cartridge (C18 extraction column, United Chemical Technologies, Inc.) at the flow rate of 50 mL min^{-1}. The cartridges were pretreated with 100 mL of high purity methanol followed by 50 mL of acidified (pH 2) Milli-Q water prior to extraction. After extraction each cartridge was rinsed with 1 L of acidified (pH 2) Milli-Q water to remove salts and stored in the refrigerator (4 °C) until further processing. The extracted material was eluted from the C18 cartridges with high purity methanol and evaporated to dryness using a rotary evaporator at 30−35 °C. The dried material was redissolved in a few milliliters of Milli-Q water, adjusted to pH 7 with a dilute NaOH solution and stored frozen until further analysis. Hereafter, these samples are referred to as either the C18 or MAB extracts.

Apparatus. Hewlett-Packard 8452A and Shimadzu 2401-PC spectrophotometers were used to acquire UV−visible absorption spectra from 190 to 820 nm. Steady-state emission

* Address correspondence to either author. E-mail: neilb@umd.edu (N.V.B.); rossdv@umd.edu (R.D.V.).
[†] Department of Chemistry and Biochemistry.
[‡] Earth System Science Interdisciplinary Center.

10.1021/es803264g CCC: $40.75
Published on Web 03/02/2009

TABLE 1. Absorption Coefficients at 280 and 355 nm (a(280) and a(355) (m^{-1})), *S* (nm^{-1}), TLP, and GPC Retention Time (At 50% Of Total Area) for LAC, SRHA, SRFA,C18 Extracts, and CDOM[a]

Sample	Position Lon(N); Lat(W)	Salinity (ppt)	a(280) (m^{-1})	a(355) (m^{-1})	S (nm^{-1})	[b]a(280) (m^{-1})	[b]a (355) (m^{-1})	S (nm^{-1})	TLP (μg/L)	GPC (min)
SRFA (1 mg/l)			3.25	1.36	0.015				2.9±0.8[c]	16.9
SRHA (1 mg/l)			5.33	2.68	0.012				2.7±0.3[c]	15.1
LAC-total (1 mg/l)			3.17	1.14	0.017				15.2±2.9[c]	14.0
LAC-F2			62.3	21.1	0.017				NA	NA
LAC-F6			41.3	13.1	0.018				NA	NA
			CDOM	*CDOM*	*CDOM*	*C18*	*C18*	*C18*	*C18*	*C18*
1. MDB_2m_(06)	39.3;-75.4	12.5	14.14	3.69	0.018	4.79	1.45	0.017	4.8±0.60	21.1
2. Shelf_2m_(06)	38.2;-74.3	31.5	2.09	0.31	0.023	0.59	0.16	0.020	1.1±0.20	23.4
3. Shelf_35m_(06)	38.2;-74.3	33.1	1.75	0.39	0.018	0.49	0.16	0.015	0.9±0.10	19.6
4. GS_2m_(06)	36.2;-71.8	36.1	0.50	0.06	0.033	0.11	0.02	0.025	0.5±0.30	23.0
5. GS_1000m_(06)	36.2;-71.8	35.1	0.49	0.08	0.018	0.10	0.03	0.016	0.5±0.40	21.8
6. MDB_2m_(05)	39.3;-75.4	14.4	13.25	3.44	0.017	5.84	1.85	0.016	7.1±0.90	23.0
7. Shelf_2m_(05)	38.2;-74.2	32.5	1.55	0.22	0.024	0.32	0.06	0.022	0.7±0.16	NA
8. Shelf_43m_(05)	38.2;-74.2	32.5	1.81	0.41	0.019	0.52	0.15	0.016	0.8±0.02	NA

[a] $a(\lambda) = 2.303A/l$, where l is the optical pathlength in meters. *S* (eq 1) values have uncertainty ≈ 0.001. NA, data not available. [b] $a(\lambda)$ for C18 extracts have been normalized to the volume of the extracted water; thus a comparison with CDOM provides a measure of the overall yield of the extraction (ie. extraction efficiency plus losses in all subsequent steps). [c] TLP in μg/mg material digested.

spectra were obtained with an Aminco-Bowman AB-2 luminescence spectrometer with excitation and emission bandpasses set to 4 nm. Time-resolved emission decays were acquired with a home-built time-correlated single photon counting spectrometer (*23*), capable of resolving lifetimes down to ~20 ps. A mode-locked Wideband Mai-Tai (Newton Corp.) titanium sapphire laser provided pulses that were frequency-doubled to achieve a wavelength range of 385−440 nm. Bin width was set to 12 ps. The instrument response function (IRF) exhibited a full width at half-maximum of ~50 ps.

Relative average molecular sizes were obtained by gel permeation chromatography (GPC) using a 1.5 × 43.5 cm G-25 Sephadex column (Aldrich) and an eluant of 5 mM phosphate buffer (pH 7), 5 mM NaCl at a flow rate of 1 mL/min. A World Precision Instruments UV/vis spectrometer (TIDAS 9.5) was used to monitor the absorption at 280 nm employing a 2 cm path length fiber optic cell (100 μL internal volume). Elution profiles were normalized to unit area, with average size then estimated as the retention time corresponding to equal areas under the elution profile, with longer retention times corresponding to smaller average size.

Procedure. Absorption and emission spectra of the MAB extracts were obtained in either MQ water (pH 7.0) or 10 mM phosphate buffer (pH 7.0) as previously described (*4, 8, 10, 24*). Values of the spectral slope parameter (*S*) were obtained from a nonlinear least-squares fit of the absorption spectra to an exponential function over the range from 300 to 700 nm (*4*),

$$a(\lambda) = a(\lambda_0)e^{-S(\lambda-\lambda_0)}, \quad (1)$$

where $a(\lambda)$ is the absorption coefficient, *S* is the spectral slope, and λ_0 is the reference wavelength.

Due to sample limitations, the detailed spectral dependence of λ_{max} and ϕ were acquired only for the 2006 samples. Values of λ_{max} and ϕ were obtained as previously reported (*8*).

Samples for emission lifetime measurements were adjusted to an absorbance of 0.100 ± 0.005 at 400 nm in 10 mM phosphate buffer, pH 7. Emission decays of SRFA and SRHA were collected at excitation wavelengths of 385, 400, and 440 nm employing a series of long pass emission filters with wavelengths of 50% transmittance greater than λ_{exc} (see Figure 1). All MAB extracts were excited at 385 and 440 nm, except GS_1000m_ (06), which was excited only at 385 nm. An IRF was collected periodically using a dilute solution of coffee creamer (~0.7 mg/mL) to scatter light into the detector in the absence of an emission filter. Data were collected until the peak channel count reached 10 000.

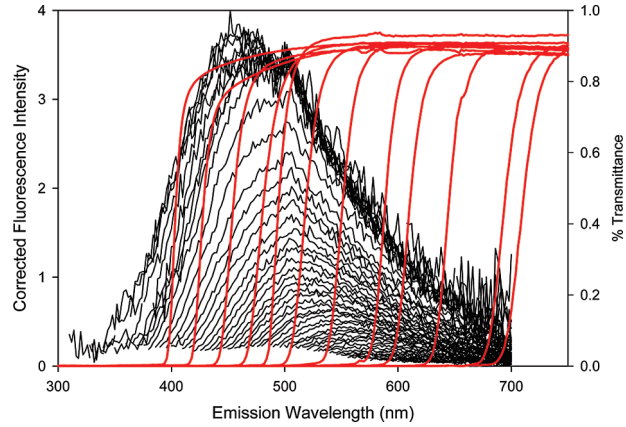

FIGURE 1. Corrected emission spectra (λ_{em} = 300−700 nm) of SRHA (black lines) from λ_{ex} = 300−600 nm. Overlaid are the transmittance profiles of all long-pass filters used in the time-resolved emission measurements (red lines).

All decays were deconvoluted (*23*) using the most recent IRF, and fit to a triple exponential decay,

$$I(t) = \sum_{i=1}^{3} \alpha_i e^{-t/\tau_i} \quad (2)$$

where $I(t)$ is the total emission intensity at time *t*, α_i is the fractional amplitude of *i*th component, and τ_i is the lifetime of *i*th component.

Eight parameters (six within the decay, as well as x-offset and background) were optimized iteratively in a least-squares

fitting program to yield the best χ^2's (<3). The fractional emission contribution of each component (f_i) to the total steady-state emission intensity was calculated as

$$f_i = \frac{\alpha_i \tau_i}{\sum_{k=1}^{3} \alpha_k \tau_k} \quad (3)$$

while the mean lifetime (τ_m) for each decay was computed as

$$\tau_m = \sum_{i=1}^{3} f_i \tau_i. \quad (4)$$

Total lignin phenol content (TLP) was determined using a modified version of the CuO method (*25*−*27*). Samples were digested in a microwave system (CEM MARS-5) and analyzed by gas chromatography employing a Shimadzu GC-17A containing a 60 m × 0.23 mm (I.D.) × 0.25 μm film thickness column (J&W DB-1) and flame ionization detection. TLP corresponds to the sum of vanillin, acetovanillone, vanillic acid, syringaldehyde, acetosyringone, syringic acid, p-coumaric acid, and ferulic acid.

Results

Spectral Dependence of Absorption, Emission Maxima and Emission Quantum Yields; Relation to Lignin Phenol Content and Molecular Size. The values of *S* obtained from the fits of the absorption spectra are provided in Table 1 for both the natural waters (CDOM) and the C18 extracts obtained from these waters. The values of *S* acquired for offshore surface waters were higher than those observed for waters below the thermocline or in the Bay and increased with increasing offshore distance, consistent with a photochemical modification of CDOM in the mixed layer over the summertime as seen in earlier studies (*28, 29*). The slightly lower values of *S* obtained for the C18 extracts can be attributed to a preferential enrichment of longer wavelength absorbing material as previously demonstrated (*24*). Except for LAC, *S* increased with decreasing size as determined by relative retention times in GPC; while *S* increased in the order SRHA < SRFA< MAB extracts, the opposite trend in relative size was observed (Table 1). Among the MAB extracts, offshore surface waters exhibited the lowest absorption coefficients, highest *S* and the smallest average size.

Absorption coefficients at 280 and 355 nm were highly correlated with TLP for both CDOM and the C18 extracts of MAB (Table 1 and Figure S1 of the Supporting Information(SI)) consistent with prior work (*19, 30, 31*). While SRHA and SRFA also exhibited a similar relationship between absorption and TLP, LAC surprisingly exhibited much higher TLP relative to its absorption (Table 1 and SI Figure S1). The possible causes of this difference are discussed below.

All samples exhibited a very similar dependence of λ_{max} and ϕ on λ_{ex} (Figure 2). For λ_{ex} < 375 nm, ϕ decreased with decreasing λ_{ex}, while in most cases λ_{max} remained relatively constant. Only the surface water samples collected offshore (2_Shelf_2m_(06) and 4_GS_2m_(06)) showed a continuous shift of λ_{max} to shorter wavelengths with decreasing λ_{ex} over this range. For all samples, excitation at wavelengths <375 nm gave rise to a very broad emission that extended well into the red, encompassing those wavelengths where emission was observed at all longer λ_{ex} (>375 nm), as shown for SRHA in Figure 1. Above $\lambda_{ex} \approx 375$ nm, λ_{max} shifted continuously to the red with increasing λ_{ex}, while the ϕ decreased monotonically (Figures 1 and 2).

While relative size decreased in the order LAC > SRHA > SRFA > MAB extracts, ϕ increased (Table 1; Figure 2). Separation by GPC of LAC into small and large molecular size fractions also showed that ϕ increased substantially in the smaller size fraction, although the spectral dependence of ϕ remained similar (SI Figure S2).

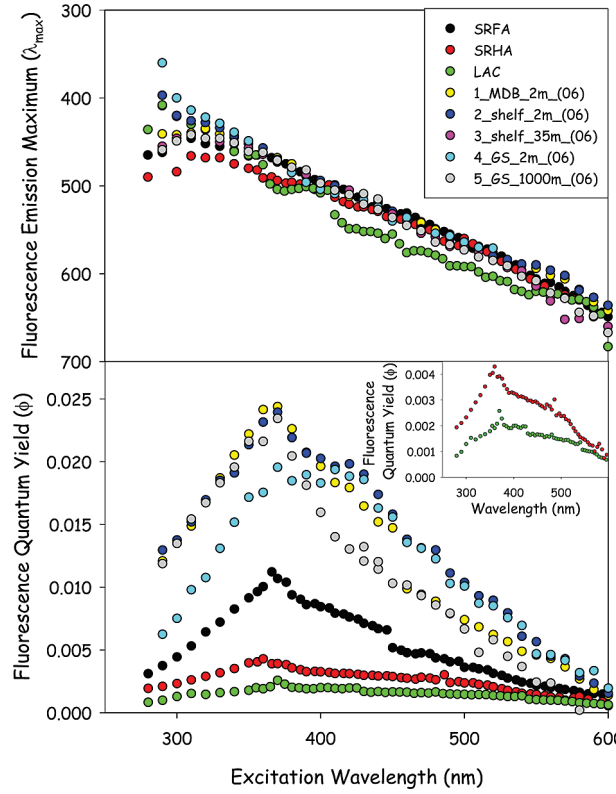

FIGURE 2. Wavelength dependence of emission maxima (top panel) and quantum yields (bottom panel) (λ_{ex} = 280−600 nm) for LAC, SRHA, SRFA, and the MAB extracts. Inset: enlarged scale for LAC and SRHA emission quantum yields.

Spectral Dependence of the Time-Resolved Emission. Although the decays of all samples were quite rapid and complex, a clear trend was evident in the overall rates of decay, which decreased in the order LAC > SRHA > SRFA> MAB extracts (Figure 3), consistent with the increase in ϕ with decreasing molecular size reported above. For all samples, the rapidity of the decay increased as shorter emission wavelengths were removed by the use of successively longer wavelength filters (beyond ~475 nm), indicating increasingly more rapid relaxation toward the red edge of the emission. This emission extended beyond the visible and into the near-infrared (>715 nm).

Decays were fit to a sum of three exponentials to acquire estimates of the lifetimes and their variation with wavelength. Although the decays were complex and only approximated by a triple exponential form (SI Figure S3), this model was chosen over more complicated forms not only for its relative simplicity, but also for comparison to past studies (*32*−*35*; SI Figures S4−S21).

For all samples, the decays were dominated by a very short-lived component (τ_{short} <150 ps, α_{short} between 50 and 90%; SI Figures S4−S21). Much smaller contributions to the total decay amplitude were observed for the intermediate lifetime component (τ_{int} between 0.3 and 1.3 ns, α_{int} between 5 and 30%), whereas the smallest contribution was observed for the longest lifetime component (τ_{long} between 2 and 5.5 ns, α_{long} between 2 and 18%). Importantly, although the shortest-lived components dominated the total population of emitting species (largest α), their contribution to the steady-state fluorescence intensity (f_i) was the least (SI Figures S4−S21), illustrating that steady-state emission spectra grossly misrepresent the abundance and importance of these

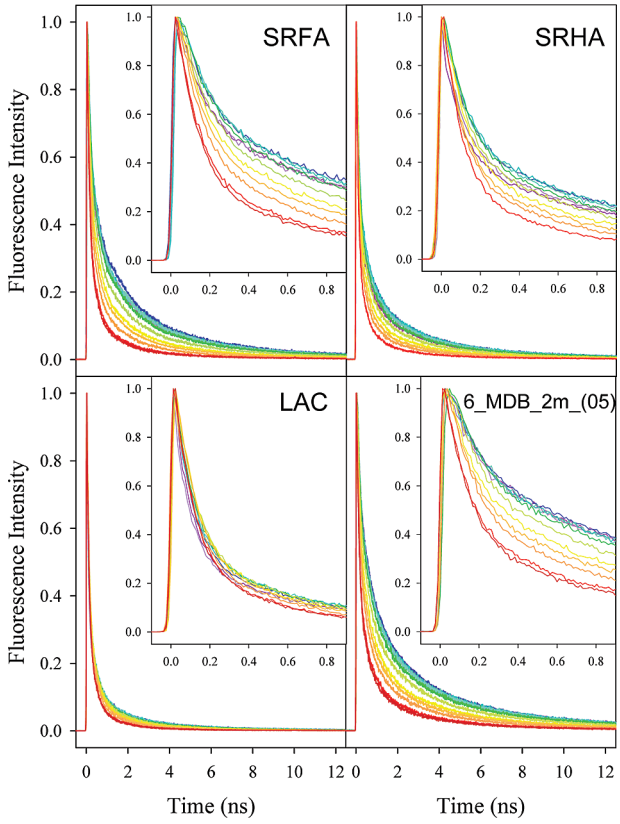

FIGURE 3. Spectral dependence of the emission decays at λ_{ex} = 385 nm obtained using a series of long-pass emission filters (Figure 1) for SRFA, SRHA, LAC, and 6_MDB_2m_(05).

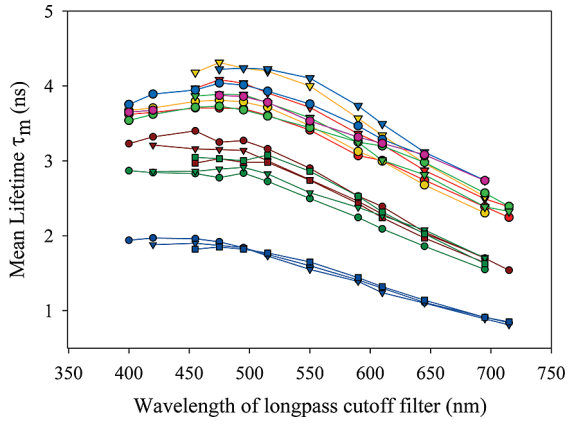

FIGURE 4. Wavelength dependence of mean lifetimes for LAC, SRHA, SRFA, and the MAB extracts at λ_{ex} from 385 to 440 nm. Values on the *x*-axis correspond to the wavelength of 50% transmittance of the long-pass emission filters.

short-lived species to the photophysical properties of these materials (eq 3) (*4, 33, 35*).

The lifetime and amplitude of all components varied as the wavelength of the long-pass filters was increased (SI Figures S4−S21). With few exceptions, beyond ~475 nm, τ_{short} remained constant or slightly decreased, whereas α_{short} significantly increased; both α and τ for the intermediate and long-lifetime components decreased, clearly reflecting the much more rapid relaxation at the successively longer wavelengths on the red edge of the emission (Figure 3).

Mean lifetimes, which provide a simpler way of illustrating the overall decay variations, exhibited three main patterns (Figure 4). First, τ_m increased in the same order as ϕ (Figure 2), with LAC < SRHA < SRFA < MAB extracts. This trend is opposite to the trend in molecular size (Table 1), indicating that more rapid decay is occurring within the larger molecules. Variations in τ_m (and ϕ) among the MAB extracts were much smaller, making it more difficult to discern obvious trends within these samples. Second, τ_m exhibited either no change or a slight increase with increasing wavelength of the long-pass filter up to ~475 nm, while beyond this wavelength, τ_m of all samples decreased monotonically with increasing wavelength. Third, varying λ_{ex} from 385 to 440 nm produced very little change in the spectral dependence of τ_m for LAC, SRHA and SRFA, while only slight increases in τ_m were observed with λ_{ex} = 440 nm for the MAB extracts (<15%), and these values tended to converge at longer emission wavelengths (Figure 4).

Discussion

We previously provided evidence that the absorption and emission spectra of HS could not result solely from a simple summation of the spectra of numerous electronically isolated chromophores (*8*). Instead, these optical properties were proposed to result in part from intramolecular charge-transfer interactions between hydroxy-aromatic donors and quinoid or other acceptors formed by the partial oxidation of lignin precursors. The results presented here, combined with prior observations, support and extend these conclusions.

First, numerous lines of evidence implicate a strong linkage between the optical properties of humic substances and partially oxidized forms of lignin. Extracted lignins, like the HS and MAB extracts, exhibit an absorption tail that extends well across the visible wavelengths (Table 1, SI Figure, and refs *36, 37*). Early work by Furman and Lonsky (*36, 37*) on kraft lignin provided evidence that charge-transfer interactions were a major contributor to this long wavelength absorption, while more recently, Barsberg et al. (*38*) also presented evidence that these interactions contribute to the absorption of visible light by lignins. As shown here, the spectral dependence of ϕ, λ_{max}, and τ_m is very similar both for extracted lignin (LAC) and for the HS and MAB extracts (Figures 2 and 4; SI Figure S2), implicating a common photophysical and thus structural basis for these properties. Our data (Table 1), as well as others (*19, 30, 31*), indicate that absorption by humic substances and CDOM is highly correlated with TLP, while the results of ultrahigh resolution mass spectrometry (Fourier transform ion cyclotron resonance; FT ICR) indicate that lignin-derived structures represent a significant component of SRFA (*39, 40*) and of C18 extracts obtained in the MAB (*41*).

These results lead us to conclude that the optical properties commonly associated with terrestrial HS and CDOM arise primarily from an ensemble of partially oxidized lignins derived from vascular plant sources. Although other partially oxidized hydroxy-aromatics such as the tannins could also produce these optical properties in principle (*8, 41, 42*), their contribution appears to be nominal at least in most aquatic environments (*42*). Further, while evidence for the formation of humic substances and CDOM from nonvascular plant sources in aquatic environments has been reported (*4, 5, 43, 44*), these materials usually exhibit much lower aromatic content (*44*), much less or no absorption in the visible (larger S (*43*)) or discrete bands (*45*), making it unlikely that their optical properties originate from the same structural basis (*44*).

Second, our results, like those of many previous studies (eg., refs *3, 4, 22, 44−49,*), indicate that the average molecular size of the ensemble is an important determinant of the optical properties. The strong decrease of ϕ and τ_m with increasing average size (Figures 2, 4, and SI Figure S2) as well as the extreme rapidity of the emission decays, especially on the red edge (Figures 3, 4, and SI Figures S4−S21), indicate that intramolecular electronic interactions must be playing

an important role in the very rapid relaxation of the excited states back to the ground states within these materials. Consistent with this view, prior work has shown that higher molecular weight HS and CDOM exhibits both a lower efficiency of photosensitization (*50, 51*) and much faster relaxation of absorption transients in laser flash photolysis experiments (*52*). Prior work has also shown a general trend of decreasing S with increasing average molecular size (Table 1 and refs *3, 4, 22, 47)* that we previously interpreted as due to the larger number and variety of charge-transfer contacts that could be potentially formed within the larger molecules of the ensemble (*8*). Although this general trend with size also holds true in this study (Table 1), LAC represents a key exception because of its very high molecular weight ($MW_w \sim 175\,000$, $MW_n \sim 16\,000$) and relatively high value of S. This result suggests that other factors in addition to size, such as the degree of oxidation (*36, 37, 44*) and differences in the original monomer content of the lignin source, are also likely to be important determinants of the optical properties. We believe that these two factors likely play a role in the lower ratio of absorption to TLP observed for LAC (Figure 2), although a higher yield of TLP in the CuO digestion of LAC can not be excluded.

Third, the complex spectral dependence of the steady-state and time-resolved emission (Figures 2−4 and SI Figures S2−S21) cannot be reconciled with a simple superposition of a small number of independently absorbing and emitting chromophores (*9, 53−55*). The continuous shift of λ_{max} to the red and concomitant decrease in ϕ at $\lambda_{ex} > 375$ nm (Figures 1 and 3) indicates the presence of a (near-)continuum of emitting species or states (*8*). Moreover, the monotonic decrease in τ_m at successively longer emission wavelengths beyond ~475 nm (Figure 4) also indicates the presence of numerous species or states that display increasingly more rapid relaxation with decreasing energy (Figure 3, 4, and SI Figures S4−S21). These results are consistent with our prior assignment of this long wavelength emission to recombinational luminescence arising from a distribution of lower energy charge-transfer states within the larger molecules of the size ensemble; as the energy of these states decreases, nonradiative relaxation would be expected to increase relative to the radiative rate (*8*), thus leading to the monotonic decrease in ϕ (Figure 2) and τ_m (Figure 4) on the red edge of the absorption and emission, respectively.

Emission spectra acquired at longer λ_{ex} always fell within the emission envelope of spectra acquired at shorter λ_{ex} (eg., Figure 1), implying that the emitting species populated by longer wavelength excitation are a lower energy subset of those populated by shorter wavelength excitation (*8*). Although λ_{ex} could be varied by only 55 nm (from 385 to 440 nm) due to limitations of the laser source, the observation that the wavelength dependence of τ_m (and the 3-exponential fits) is largely independent of λ_{ex} is also consistent with this conclusion (Figure 4 and SI Figures S4−21). Only a few of the MAB extracts exhibited values of τ_m that were slightly higher at $\lambda_{ex} = 440$ nm (<15%), and it is unclear, given the uncertainties in the fitting, whether these differences are real. These results thus provide further evidence that the emission spectra from these materials originate from a coupled manifold of states (*8*). They further suggest that the same red emissive states can be populated by excitation at both short (<385 nm) and long (>385 nm) wavelengths (Figures 1 and 4), although with an efficiency that depends on λ_{ex} (Figure 2).

Based on these observations, the following tentative model is suggested. At $\lambda_{ex} < 375$ nm, where the absorption should be increasingly dominated by the known aromatic structures within lignin (local states, refs *56, 57)*, the observed emission is proposed to arise from a superposition of emission from the local states (blue edge, less than ~470 nm (*57*)) and the charge-transfer states (red edge, greater than ~470 nm). Population of the red emissive charge-transfer states by short wavelength excitation into the local states ($\lambda_{ex} < 375$ nm) requires a mechanism. Two possible mechanisms are (1) intramolecular excited-state electron transfer from local donor states to either quinoid or other electron acceptors, and (2) energy transfer from the local states to the charge-transfer states. Quenching at short λ_{ex} could also occur in part via energy transfer from higher to lower energy local states. Because a substantial Stoke's shift is observed with very short λ_{ex} (eg., 300 nm) for many but not all of the samples (Figures 1 and 3), energy transfer is likely to be occurring in some cases. Consistent with the decrease in ϕ at $\lambda_{ex} < 375$ nm (Figure 2), Frimmel and Kumke (*34*) observed for a number of natural water samples that τ_m decreased with decreasing wavelength on the blue edge of the emission spectrum obtained by short-wavelength excitation ($\lambda_{ex} = 314$ nm), and interpreted their data as due to quenching by energy transfer. Thus, the decrease in ϕ and the presence of long wavelength emission with $\lambda_{ex} < 375$ nm can be explained by a combination of two factors: (1) rapid intramolecular quenching of the local states by energy and/or electron transfer, and (2) population of the lower energy charge-transfer states via these mechanisms, but with low efficiency.

As λ_{ex} approaches 375 nm, the enhanced ϕ is suggested to arise from an increasingly greater emission contribution from charge-transfer states populated by direct excitation. Beyond $\lambda_{ex} \sim 375$ to 400 nm, where the local donor states should no longer absorb, the absorption and emission is primarily attributed to an ensemble of charge-transfer states of differing energies, with ϕ decreasing with increasing λ_{ex} due to more rapid nonradiative relaxation at decreasing energies (see above).

Consistent with current experimental evidence (*4*), this model predicts that S will increase with decreasing average molecular size due primarily to the lower probability of forming charge-transfer contacts within the smaller-sized molecules. Enhanced, blue-shifted emission arising from the local states would also be expected with decreasing average size owing to fewer intramolecular quenching interactions as well as a lesser contribution from the charge-transfer states.

Interestingly, the spectral dependence of the quantum yields for formation of a number of the major photochemical products (eg., H_2O_2, CO and CO_2) and processes (photobleaching) exhibits an inverse relationship with ϕ below ~400 nm (Figure 2 and refs *10, 58−60*). This result suggests that at least some part of the emission quenching below 400 nm leads to photochemistry, possibly through excited-state electron transfer (see above), or through direct photochemistry of the local states particularly at very short wavelengths (<310 nm; *56, 57, 61, 62*). In contrast, however, smaller size fractions exhibit both enhanced emission intensity and photosensitization efficiency (Figure 2 and refs *50, 51*). These results suggest that size may play a key role in determining the importance of particular photochemical pathways.

Acknowledgments

We thank Prof. Doug English and Dr. Amy Grimes for assistance with laser operation, Jeanne Yang and Tammi Pisano with the TLP analyses, and Alexie Jullien and Laure Arabia with the GPC analyses. This work was supported by grants from the National Science Foundation (OCE-0443217 and OCE-0648414) to NVB and RDV.

Supporting Information Available

Dependence of absorption coefficients on TLP (Figure S1), spectral dependence of λ_{max} and ϕ for a small and large size fraction of LAC (Figure S2), a representative fit of an emission decay to a 3-exponential function (Figure S3), and spectral dependence of the lifetimes and amplitudes of the decay

components for all samples (Figures S4−S21). This material is available free of charge via the Internet at http://pubs.acs.org.

Literature Cited

(1) Bricaud, A.; Morel, A.; Prieur, L. Absorption by dissolved organic matter of the sea (yellow substance) in the UV and visible domains. *Limnol. Oceanogr.* **1981**, *26*, 43–53.

(2) Zepp, R. G.; Schlotzhauer, P. F. Comparison of photochemical behavior of various humic substances in water. 3. Spectroscopic properties of humic substances. *Chemosphere* **1981**, *10*, 479–486.

(3) Blough, N. V.; Green, S. A. Spectroscopic characterization and remote sensing of non-living organic matter. In *The Role of Non-living Organic Matter in the Earth's Carbon Cycle*; Zepp, R. G., Sonntag, C., Eds.; Wiley: Chichester, UK, 1995; pp 23−45.

(4) Blough, N. V.; Del Vecchio, R. Chromophoric DOM in the coastal environment. In *Biogeochemistry of Marine Dissolved Organic Matter*; Hansel, D. A., Carlson, C. A., Eds.; Academic Press: San Diego, 2002; pp 509−546.

(5) Nelson, N. B.; Siegel, D. A. Chromophoric DOM in the open ocean. In *Biogeochemistry of Marine Dissolved Organic Matter*; Hansel, D. A., Carlson, C. A., Eds.; Academic Press: San Diego, 2002; pp 547−578.

(6) Del Castillo, C. E. *In Remote Sensing of Coastal Aquatic Environments*; Miller, R. L., Del Castillo, C. E., McKee, B. A., Eds.; Springer: Dordrecht, The Netherlands, 2005.

(7) Coble, P. G. Optical biogeochemistry: The chemistry of ocean color. *Chem. Rev.* **2007**, *107*, 402–418.

(8) Del Vecchio, R.; Blough, N. V. On the origin of the optical properties of humic substances. *Environ. Sci. Technol.* **2004**, *38*, 3885.

(9) Ma, X.; Green, S. A. Fractionation and spectroscopic properties of fulvic acid and its extract. *Chemosphere* **2008**, *72*, 1425–1434.

(10) Del Vecchio, R.; Blough, N. V. Photobleaching of chromophoric dissolved organic matter in natural waters: Kinetics and modeling. *Mar. Chem.* **2002**, *78*, 231–253.

(11) Goldstone, J. V.; Del Vecchio, R.; Blough, N. V.; Voelker, B. M. A multicomponent model of chromophoric dissolved organic matter photobleaching. *Photochem. Photobiol.* **2004**, *80*, 52–60.

(12) Kujawinski, E. B.; Del Vecchio, R.; Blough, N. V.; Klein, G. C.; Marshall, A. G. Probing molecular-level transformations of dissolved organic matter: insights on photochemical degradation and protozoan modification of DOM from electrospray ionization Fourier transform ion cyclotron resonance mass spectrometry. *Mar. Chem.* **2004**, *92*, 23–37.

(13) Power, J. F.; Langford, C. H. Optical absorbance of dissolved organic matter in natural water studies using the thermal lens effect. *Anal. Chem.* **1988**, *60*, 842–846.

(14) Jones, G.; Indig, G. L. Spectroscopic and chemical binding properties of humic acids in water. *New J. Chem.* **1996**, *20*, 221–232.

(15) Ariese, F.; van Assema, S.; Gooijer, C.; Bruccoleri, A. G.; Langford, C. H. Comparison of laurentian fulvic acid luminescence with that of the hydroquinone/quinone model system; evidence from low temperature fluorescence studies and EPR spectroscopy. *Aquat. Sci.* **2004**, *66*, 86–94.

(16) Korshin, G. V.; Kumke, M. U.; Li, C. W.; Frimmel, F. H. Influence of chlorination on chromophores and fluorophores in humic substances. *Environ. Sci. Technol.* **1999**, *33*, 1207–1212.

(17) Michaelis, L.; Granick, S. Molecular compounds of the quinhydrone type in solution. *J. Am. Chem. Soc.* **1944**, *66*, 1023–1030.

(18) Kumke, M. U.; Frimmel, F. H.; Ariese, F.; Gooijer, C. Fluorescence of humic acids (HA) and pyrene-HA complexes at ultralow temperature. *Environ. Sci. Technol.* **2000**, *34*, 3818–3823.

(19) Hernes, P. J.; Benner, R. Photochemical and microbial degradation of dissolved lignin phenols: Implications for the fate of terrigenous dissolved organic matter in marine environments *J. Geophys. Res., [Oceans]* **2003***108*3291, DOI: 3210.1029/2002JC001421.

(20) Kamogawa, H.; Giza, Y. C.; Cassidy, H. G. Electron transfer polymers. 23. Interactions of quinhydrone type in polyvinylhydroquinone solutions. *J. Polym. Sci., Part A: Polym. Chem.* **1964**, *2*, 4647.

(21) Moser, R. E.; Cassidy, H. G. Electron transfer polymers. 27. Solvent effects on absorption spectra of partially oxidized oligomeric hydroquinones. *J. Org. Chem.* **1965**, *30*, 3336.

(22) Chin, Y. P.; Aiken, G.; O'Loughlin, E. Molecular weight, polydispersity, and spectroscopic properties of aquatic humic substances. *Environ. Sci. Technol.* **1994**, *28*, 1853–1858.

(23) Grimes, A. F.; Call, S. E.; Vicente, D. A.; English, D. S.; Harbron, E. Toward efficient photomodulation of conjugated polymer emission: Optimizing differential energy transfer in azobenzene-substituted PPV derivatives. *J. Phys. Chem. B* **2006**, *110*, 19183–19190.

(24) Green, S. A.; Blough, N. V. Optical absorption and fluorescence properties of chromophoric dissolved organic matter in natural waters. *Limnol. Oceanogr.* **1994**, *39*, 1903–1916.

(25) Hedges, J. I.; Ertel, J. R. Characterization of lignin by gas capillary chromatography of cupric oxide oxidation products. *Anal. Chem.* **1982**, *54*, 174–178.

(26) Goni, M. A.; Montgomery, S. Alkaline CuO oxidation with a microwave digestion system: Lignin analyses of geochemical samples. *Anal. Chem.* **2000**, *72*, 3116–3121.

(27) Louchouarn, P.; Opsahl, S.; Benner, R. Isolation and quantification of dissolved lignin from natural waters using solid-phase extraction and GC/MS. *Anal. Chem.* **2000**, *72*, 2780–2787.

(28) Vodacek, A.; Blough, N. V.; DeGrandpre, M. D.; Peltzer, E. T.; Nelson, R. K. Seasonal variation of CDOM and DOC in the Middle Atlantic Bight: Terrestrial inputs and photooxidation. *Limnol. Oceanogr.* **1997**, *42*, 674–686.

(29) Del Vecchio, R.; Blough, N. V. Spatial and seasonal distribution of chromophoric dissolved organic matter and dissolved organic carbon in the Middle Atlantic Bight. *Mar. Chem.* **2004**, *89*, 169–187.

(30) Spencer, R. G. M.; Aiken, G. R.; WicklandK. P. StrieglR. G. Hernes, P. J. Seasonal and spatial variability in dissolved organic matter quantity and composition from the Yukon River basin, Alaska *Global Biogeochem. Cycles* **2008** *22*GB4002 DOI: 10.1029/2008GB003231.

(31) Hernes, P. J.; Spencer, R. G. M.; Dyda, R. Y.; Pellerin, B. A.; Bachand, P. A. M.; Bergamaschi, B. A. The role of hydrologic regimes on dissolved organic carbon composition in an agricultural watershed. *Geochim. Cosmochim. Acta* **2008**, *72*, 5266–5277.

(32) Cook, R. L.; Langford, C. H. Metal ion quenching of fulvic acid fluorescence intensities and lifetimes: Non-linearities and a possible three-component model. *Anal. Chem.* **1995**, *67*, 174–180.

(33) Herbelin, S. E. Photophysics and photochemistry of natural waters with emphasis on radical probe development and application. Masters Thesis. MIT/WHOI, 1994.

(34) Frimmel, F. H.; Kumke, M. U. Fluorescence decay of humic substances. A comparative study. In *Humic Substances: Structure, Properties and Uses*; Davies, G., Ghabour, E., Eds.; Royal Society of Chemistry: Cambridge, 1998; pp 113−122.

(35) Clark, C. D.; Jiminez-Morais, J.; Jones II, G. J.; Zanardi-Lamardo, E.; Moore, C. A.; Zika, R. G. A time-resolved fluorescence study of dissolved organic matter in a riverine to marine transition zone. *Mar. Chem.* **2002**, *78*, 121–135.

(36) Furman, G. S.; Lonsky, W. F. W. Charge-transfer complexes in kraft lignin. 1. Occurrence. *J. Wood Chem. Technol.* **1988**, *8*, 165–169.

(37) Furman, G. S.; Lonsky, W. F. W. Charge-transfer complexes in kraft lignin: Contribution to color. *J. Wood Chem. Technol.* **1988**, *8*, 191–208.

(38) Barsberg, S.; Elder, T.; Felby, C. Lignin-quinone interactions: Implications for optical properties of lignin. *Chem. Mater.* **2003**, *15*, 649–655.

(39) Stenson, A. C.; Marshall, A. G.; Cooper, W. T. Exact masses and chemical formulas of individual Suwannee River fulvic acids from ultrahigh resolution electrospray ionization Fourier transform ion cyclotron resonance mass spectra. *Anal. Chem.* **2003**, *75*, 1275–1284.

(40) Kujawinski, E. B.; Del Vecchio, R.; Blough, N. V.; Klein, G. C.; Marshall, A. G. Probing molecular-level transformations of dissolved organic matter: Insights on photochemical degradation and protozoan modification of DOM from electrospray ionization Fourier transform ion cyclotron resonance mass spectrometry. *Mar. Chem.* **2004**, *92*, 23–37.

(41) Sleighter, R. L.; Hatcher, P. G. Molecular characterization of dissolved organic matter (DOM) along a river to ocean transect of the lower Chesapeake Bay by ultrahigh resolution electrospray ionization Fourier transform ion cyclotron resonance spectrometry. *Mar. Chem.* **2008**, *110*, 140−152.

(42) Maie, N.; Pisani, O.; Jaffé, R. Mangrove tannins in aquatic ecosystems; Their fate and possible influence on dissolved organic carbon and nitrogen cycling. *Limnol. Oceanogr.* **2008**, *53*, 160–171.

(43) Nelson, N. B.; Siegel, D. A.; Michaels, A. F. Seasonal dynamics of colored dissolved material in the Sargasso Sea. *Deep-Sea Res., Part I* **1998**, *45*, 931–957.
(44) Fimmen, R. L.; Cory, R. M.; Chin, Y.-P.; Trouts, T. D.; Mcknight, D. M. Probing the oxidation-reduction properties of terrestrially and microbially derived dissolved organic matter. *Geochim. Cosmochim. Acta* **2007**, *71*, 3003–3015.
(45) Her, N.; Amy, G.; Mcknight, D.; Sohn, J.; Yoon, Y. Characterization of DOM as a function of MW by fluorescence EEM and HPLC-SEC using UVA, DOC, and fluorescence. *Water Res.* **2003**, *37*, 4295–4303.
(46) Green, S. A.; Morel, F. M. M.; Blough, N. V. Investigation of the electrostatic properties of humic substances by fluorescence quenching. *Environ. Sci. Technol.* **1992**, *26*, 294–302.
(47) Yacobi, Y. Z.; Alberts, J. J.; Takacs, M.; McElvane, M. Absorption spectroscopy of colored dissolved organic carbon in Georgia (USA) rivers: the impact of molecular size distribution. *J. Limnol.* **2003**, *62*, 41–46.
(48) Lou, T.; Xie, H. Photochemical alteration of the molecular weight of dissolved organic matter. *Chemosphere* **2006**, *65*, 2333–2342.
(49) Trubetskoj, O.; Trubetskaya, O.; Reznikova, O.; Afanas'eva, G. Weight and optical differences between soil humic acids fractions obtained by coupled SEC-PAGE. *Geoderma* **1999**, *93*, 277–287.
(50) Richard, C.; Trubetskaya, O.; Trubetskoj, O.; Reznikova, O.; Afanas'eva, G.; Auger, J. P.; Guyot, G. Key role of the low molecular size fraction of soil humic acids for fluorescence and photoinductive activity. *Environ. Sci. Technol.* **2004**, *38*, 2052–2057.
(51) Trubetskaya, O.; Trubetskoj, O.; Richard, C. Photodegrading properties of soil humic acids fractionated by SEC-PAGE set-up. Are they connected to absorbance. *J. Photochem. Photobiol. A* **2007**, *189*, 247–252.
(52) Wang, W.; Zafiriou, O. C.; Chan, I.-Y.; Zepp, R. G.; Blough, N. V. Production of hydrated electrons from photoionization of dissolved organic matter in natural waters. *Environ. Sci. Technol.* **2007**, *41*, 1601–1607.
(53) Stedmon, C. A.; Markager, S.; Bro, R. Tracing dissolved organic matter in aquatic environments using a new approach to fluorescence spectroscopy. *Mar. Chem.* **2003**, *82*, 239–254.
(54) Cory, R.; McKnight, D. Fluorescence spectroscopy reveals ubiquitous presence of oxidized and reduced quinones in dissolved organic matter. *Environ. Sci. Technol.* **2005**, *39*, 8142–8149.
(55) Cory, R. M.; McKnight, D. M.; Chin, Y.-P.; Miller, P.; JarosC. Chemical characteristics of fulvic acids from Arctic surface waters: Microbial contributions and photochemical transformations *J. Geophys. Res.* **2007***112*G04S51, DOI: 10.1029/2006JG000343.
(56) Lin, S. Y.; Kringstad, K. P. Photosensitive groups in lignin and lignin model compounds. *Tappi* **1970**, *53*, 658–663.
(57) Lundquist, K.; Josefsson, B.; Nyquist, G. Analysis of lignin products by fluorescence spectroscopy. *Holzforschung* **1978**, *32*, 27–32.
(58) O'Sullivan, D. W.; Neale, P. J.; Coffin, R. B.; Boyd, T. J.; Osburn, C. L. Photochemical production of hydrogen peroxide and methylhydroperoxide in coastal waters. *Mar. Chem.* **2005**, *97*, 14–33.
(59) Ziolkowski, L. A.; Miller, W. L. Variability of the apparent quantum efficiency of CO photoproduction in the Gulf of Maine and Northwest Atlantic. *Mar. Chem.* **2007**, *105*, 258–270.
(60) Johannessen, S.; Miller, W. L Quantum yield for the photochemical production of dissolved inorganic carbon in seawater. *Mar. Chem.* **2001**, *76*, 271–283.
(61) Stubbins, A.; Hubbard, V.; Uher, G.; Law, C. F.; Upstill-Goddard, R. C.; Aiken, G. R.; Mopper, K. Relating carbon monoxide photoproduction to dissolved organic matter functionality. *Environ. Sci. Technol.* **2008**, *42*, 3271–3276.
(62) Thomas-Smith, T. E.; Blough, N. V. Photoproduction of hydrated electrons from constituents of natural waters. *Environ. Sci. Technol.* **2001**, *35*, 2721–2726.

ES803264G